Struct Multidisc Optim (2014) 50:159–168
DOI 10.1007/s00158-013-1038-y

MEDICAL AND BIOENGINEERING APPLICATIONS

NURBS modeling and structural shape optimization of cardiovascular stents

Rory Clune · Denis Kelliher · James C. Robinson · John S. Campbell

Received: 12 December 2012 / Revised: 15 September 2013 / Accepted: 9 December 2013 / Published online: 26 January 2014

Abstract Cardiovascular stents have been used since the 1990s to treat atherosclerosis, one of leading causes of death in the western world, and structural optimization has led to significant improvements in stent performance. Much of the potential variation in stent geometry, however, has remained unconsidered. This paper presents a non-uniform rational basis spline (NURBS) parameterization of a stent, the inclusion of structural fatigue resistance as a design consideration, and the results of a design optimization based on response surface techniques. Results show the feasibility and merits of the NURBS approach, which models a much broader range of shapes than was previously possible. Multi-objective optimization produces a range of geometrically diverse Pareto-optimal designs; these can be used to develop future clinical design guides, accounting for the variation observed across patients. We conclude by motivating future work with increasingly complex physical modeling and optimization capabilities.

Keywords Cardiovascular stents · Structural shape optimization · NURBS

R. Clune (✉)
Massachusetts Institute of Technology,
Cambridge, MA 02139, USA
e-mail: rory.clune@gmail.com

D. Kelliher
University College Cork, Cork, Ireland
e-mail: d.kelliher@ucc.ie

J. C. Robinson · J. S. Campbell
Kepler Engineering Software Ltd., National Software
Centre, Mahon, Cork, Ireland

1 Introduction

Atherosclerosis—the stenosis (blocking) of a coronary artery causing an occlusion that restricts blood flow—can, left untreated, lead to cardiac arrest. Cardiovascular stent implantation has become a common medical intervention for the treatment of atherosclerosis, improving on the clinical limitations of angioplasty (Balcon et al. 1997).

A stent is as a mesh-like scaffold, most commonly made from ductile metal, that supports the blocked artery, This dilates the artery's lumen (inner space) and allows blood to flow freely. The stent must support the arterial wall without becoming excessively embedded in it or causing damage during deployment, both of which are linked to *restenosis*, the re-occurrence of stenosis (Bennett 2003).

A stent is initially crimped onto a balloon-tipped catheter, which is inflated once the stent is in place in the artery. Both the crimping and the inflation operations are followed by elastic rebounding. The associated large inelastic deformations provide clinical anchorage within the artery; they also cause residual stress to accumulate, affecting the stent's long-term performance. During the stent's working life, alternating systolic and diastolic blood pressures (due to heartbeat) continuously subject it to cyclical loading.

Dumoulin and Cochelin (2000) used the finite element method (FEM) to perform one of the earliest structural analyses of a balloon-expandable stent. FEM has since seen extensive use in the evaluation of stents' structural performance (e.g., Etave et al. 2001; Migliavacca et al. 2002; Lally et al. 2005). Researchers typically post-process the primary simulation responses to quantify the performance of a given stent design in a number of ways. Fatigue resistance, however, has received relatively little attention as a performance measure despite its importance for structures whose primary loading is cyclical.

The design of a stent is determined by its geometry and material (including any drug coatings) definitions; this paper concentrates on the former. Our chosen material, tantalum alloy, is commonly used for the fabrication of permanently deformable stents (Serruys 2001).

The use of shape and sizing optimization to improve stent design is relatively new. Notable early examples are provided by Atherton and Bates (2004), who compared the results of sizing optimization using a genetic algorithm and model-based robust engineering design, and Wu et al. (2008), who developed a drug-eluting stent using topology optimization. Harewood et al. (2011) used Altair's *HyperStudy*® and *HyperMorph*® in conjunction with *LS-DYNA* to carry out an extensive parametric study and to improve the design of a stent fabricated from a shape memory alloy.

A number of researchers (Timmins et al. 2007; Xiang et al. 2008; Li et al. 2009) have developed parametric geometric models to optimize stents, with various angles and lengths chosen as parameters. Although an important step towards improved stent design, this direct parameterization misses much of the possible rich variation in shape.

Non-uniform rational basis-splines (NURBS) offer a high level of local precision and overall flexibility in defining curves; for a given number of parameters, they allow optimization schemes to consider a much more extensive range of shapes than direct parameterization (Qian 2010).

Pant et al. (2011a, b) used NURBS to model stents within an optimization process, but the design variables used are not directly related to the NURBS formulation, and the geometric aspects of the work generally follow previous sizing parameter formulations.

To the best of our knowledge, Kelliher et al. (2008) was the first paper to consider direct use of NURBS parameters as design variables in a three-dimensional modeler, demonstrating the feasibility of the concept and showing a wide range of different shapes emerging from a single geometric model. The results, however, consisted only of parametric explorations of the design space rather than full optimization.

We build on that work here, with the aims of formalizing the use of NURBS to vary stent geometry in optimization of incorporating fatigue resistance theory, and of generating optimally-performing designs.

The structural characteristics of diseased blood vessels depend, in part, on the degree of the atherosclerosis, which varies from patient to patient. This makes it impractical to propose a single optimal stent design; a goal of this paper is instead to demonstrate the use of multi-objective optimization techniques in producing a range of optimal designs for various clinical settings.

Structure of paper Section 2 introduces and develops the NURBS-based geometric model for stents, and Section 3 describes the structural analysis and derivation of structural responses. These combine in a multi-objective design optimization problem; its formulation and results appear in Section 4, and conclusions are drawn in Sections 5 and 6.

2 Geometric modeling

This section describes the underlying NURBS formulation and its application to stent modeling. Key inputs to the NURBS formulation and some additional geometric parameters enable us to generate a wide range of 3-D stent geometries.

2.1 NURBS shape definition

NURBS curves are generalized basis-spline curves that form the mainstay of the modern CAD industry. Piegl and Tiller (1997) provide a good background reference, presenting all the terms used here. NURBS are a numerically stable and very flexible parametric definition of a 2-D or 3-D curve $\mathbf{C}(u)$, defined as:

$$\mathbf{C}(u) = \frac{\sum_{i=0}^{n} N_{i,p}(u) w_i \mathbf{P_i}}{\sum_{i=0}^{n} N_{i,p}(u) w_i} \tag{1}$$

where the n control points $\mathbf{P}_i$ form the control polygon of the curve; w_i are the associated weights; p is the degree of the B-spline basis functions; u is the parameter value at which to evaluate $\mathbf{C}(u)$ where $u \in U = \{0, \ldots, 0, u_{p+1}, \ldots, u_{m-p-1}, 1, \ldots, 1\}$, the non-periodic and non-uniform knot vector of length $m = n + p + 1$; and $N_{i,p}(u)$ are the pth degree B-spline basis functions defined on U.

The ith B-spline basis function is defined recursively as:

$$\begin{aligned} N_{i,p}(u) &= \frac{u - u_i}{u_{i+p} - u_i} N_{i,p}(u) + \frac{u_{i+p+1} - u}{u_{i+p+1} - u_{i+1}} N_{i+1,p-1}(u) \\ N_{i,0}(u) &= \begin{cases} 1 & u_i \le u \le u_{i+1} \\ 0 & \text{otherwise} \end{cases} \end{aligned} \tag{2}$$

Considering (1) and (2), one can control a NURBS curve in a number of ways. These are:

- **Control Polygon:** As the NURBS curve will follow the general trend of the control polygon in accordance with the convex hull property, the geometry of its n points ($\mathbf{P}_i$) is an important method of controlling the curve.
- **Weights:** Increasing the weight w_i attributed to a control point i drags the curve towards that point, and decreasing w_i drags the curve towards all the other points. Weights can also be negative, repelling the curve from the relevant control point. Large differences

between the weights attributed to adjacent points leads to high curvature.

– **Degree:** The degree of the curve (the power, p, to which the u-values are raised in the basis function) has a significant effect on the shape of the curve. As the degree increases, the curve will follow an increasingly direct route between the first and last control points. As the degree decreases, the curve tends towards the outline of the control polygon.

2.2 Generating stent geometry using NURBS

The repetitive geometry of the overall stent can be reconstructed by reflecting a single segment along the axial direction (Fig. 1). We use this segment as an appropriate representation of the overall stent and develop a strategy to geometrically model the segment using a NURBS curve to represent its centerline. Appropriate boundary conditions on the segment ends model the reflective continuity at the ends.

The fixed dimensions of the stent used in this study are: a segment axial length of 0.915 mm c\c; an outside radius of 1.5 mm; and a radial depth of 0.085 mm. There are 20 repeated segments which, when combined with a mid-plane radius of 1.458 mm, gives the mid-plane circumferential length of 0.458 mm.

The centerline of a single stent segment is represented as a NURBS curve. A control polygon with eight nodes is developed from the stent dimensions detailed above (Fig. 2). Further exploitation of the anti-symmetry of an individual stent segment means that control points $4-7$ may be generated by reflecting nodes $3-0$ through the central reflection point. Furthermore, the weights associated with the control nodes $0-4$ are numerically equal to weights $7-4$, thereby reducing the number of weights to be specified for a given curve to four.

This polygon is used to generate a 2-D centerline of representative segments. A default knot vector with 17 equally-spaced elements is used, giving a curve of degree 7. Three

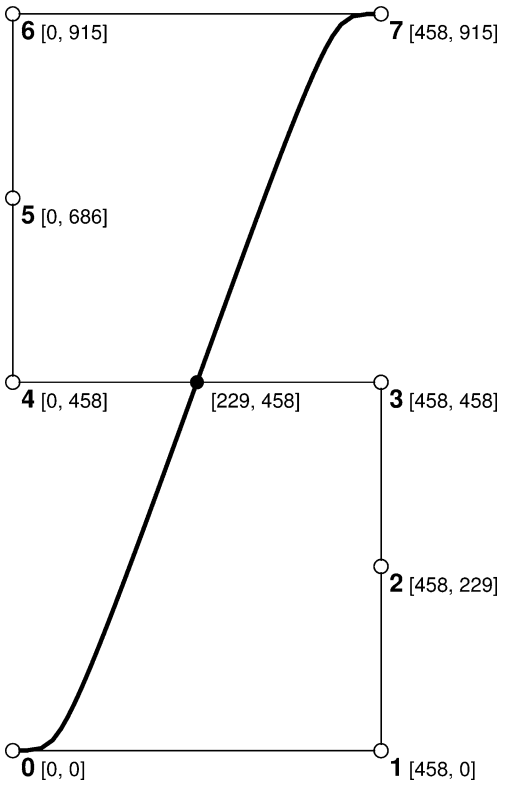

Fig. 2 Changing the geometry of the control polygon geometry has a large, but crude, effect on the NURBS curve. (Dimensions in mm)

important parameters—the control points, the knot vector, and the degree—remain fixed for the following reasons:

1. The convex hull property is used to good effect to prevent overlapping of adjacent stent segments
2. In the absence of a very large number of control points, the polygon's relatively crude and global level of control over the shape make varying its geometry an inappropriate design strategy
3. Modifying the knot intervals requires high numbers of parameters to achieve any meaningful shape variation, creating difficulties for optimization algorithms

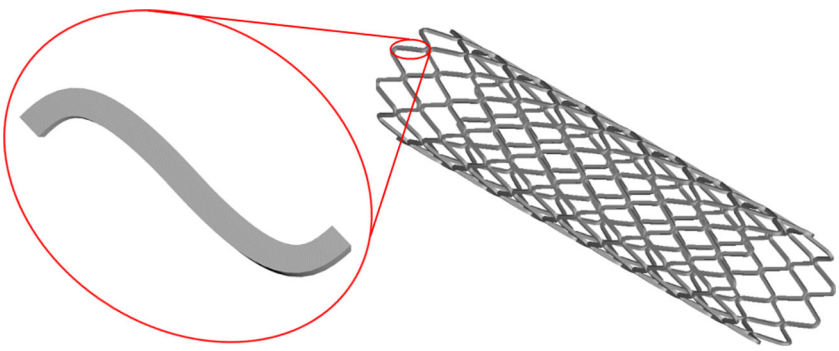

Fig. 1 Exploiting circumferential and longitudinal repetition in the stent geometry, a single segment is used in analysis and optimization to represent the overall stent

4. The degree of the curve could only be reduced and this would curb meaningful shape variation

This leaves only the weights as the means of controlling the stent shape. Since the ratio of the weights rather than the weights themselves determine a particular curve's shape, $w_0 = 1$ throughout and the remaining weights $w_i, i \in \{1, 2, 3\}$ are set as the three design variables for optimization.

The generation of the model proceeds as follows:

1. The specification of the weights $w_i, i \in \{1, 2, 3\}$ generates the stent centerline.
2. Normals are extended from the centerline at a specified thickness, which may vary along the stent (see Section 2.3).
3. These normals are then checked and subject to a filleting procedure to remove re-entrant corners, resulting in two external sets of boundary coordinates defining the external edges of the segment's mid-plane.
4. This plane of nodes is then extruded at a specified angle (see Section 2.3) to generate a 3-D set of nodes defining the finite element mesh.
5. These nodes are then mapped to cylindrical coordinates.
6. Finally, 20-node brick elements are generated for finite element analysis.

Figure 3 demonstrates a variety of shapes achieved by varying the three weights.

2.3 Additional geometric parameters

To enable an even broader range of 3-D shapes, we vary the offset thickness from the NURBS centerline in two orthogonal directions. Allowing for such thickness variation is both feasible (these stents are manufactured by laser-cutting a tantalum cylinder) and intuitively sensible (some areas along the segment will be more prone to stress concentrations and material fatigue that others and should be locally strengthened).

Two parameters, t_{mid} and t_{end}, control thickness variation along the segment's longitudinal direction (Fig. 7)

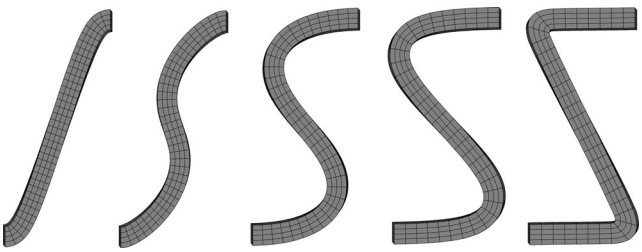

Fig. 3 Varying only the control polygon's weights leads to a rich variation in stent segment geometry

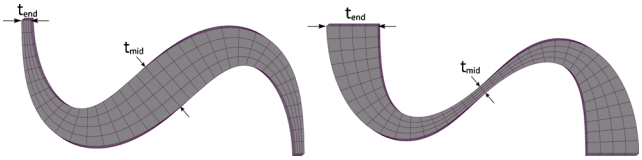

Fig. 4 Varying thickness along the segment's longitudinal direction allows for local control of material distribution

according to the kinematically admissible Hermitian curve:

$$t(d) = t_{\text{end}} + \Delta t(3d^2 - 2d^3) \qquad 0 \le d \le 1$$
$$\Delta t = t_{\text{mid}} - t_{\text{end}} \tag{3}$$

where d is the normalized distance along the segment's NURBS curve between its endpoint and midpoint. This form ensures there are no discontinuities in thickness at the segment midpoint or at the interface of segments in the overall stent (Figs. 1 and 4).

When a stent is manufactured by aligning a cutting laser along its radius, the resulting thickness will vary linearly from the inner to the outer surface of the stent (as in Fig. 5). Changing the angle of incidence of the cutting laser changes this slope of the side of the segments, θ_{side}, which we introduce as a design variable governed by:

$$t(r) = t_{\text{mid-plane}} + (r - r_{\text{mid-plane}}) \tan \theta_{\text{side}} \tag{4}$$

where $t_{\text{mid-plane}}$ and $r_{\text{mid-plane}}$ are the thickness and the radius at the mid-plane of the stent segment, and θ_{side} is measured in degrees. The initially-specified offset from the NURBS curve (Section 2.2) is interpreted as $t_{\text{mid-plane}}$.

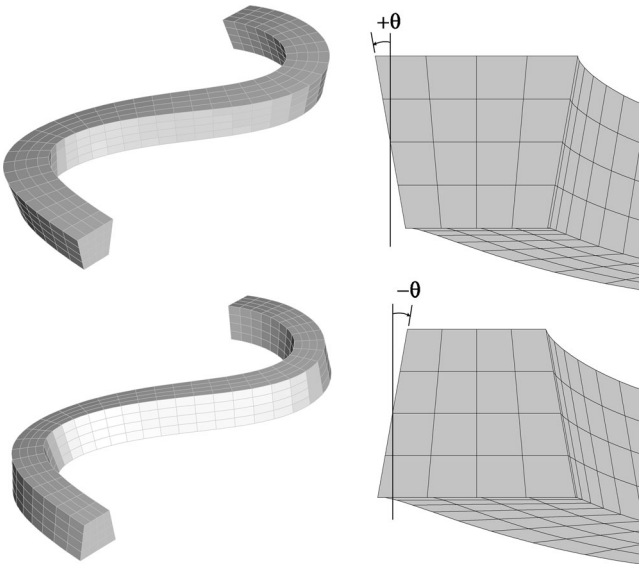

Fig. 5 Variation of the segment thickness along the stent's radius is possible with a laser-cutting manufacturing process

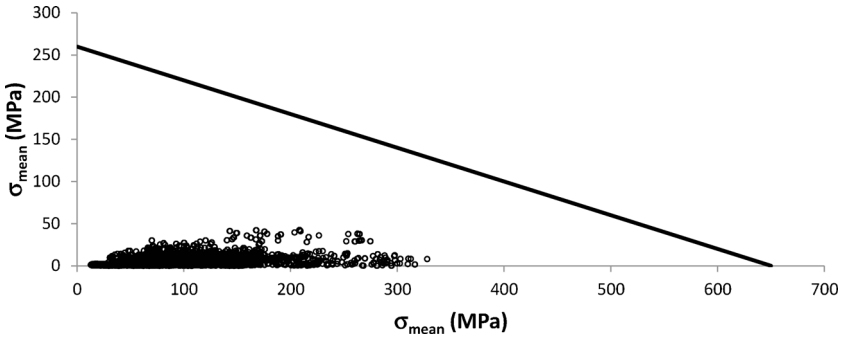

Fig. 6 The *Goodman Plot* for the design shown in Fig. 10. The *Goodman number*, our measure of fatigue resistance, is the minimum perpendicular distance from any point to the line; the structure is said to be safe if all points lie within the Goodman line

3 Structural analysis

Once the 3-D set of nodes is generated for a given stent design, a finite element model is automatically generated for the proprietary finite element analysis system Strand7®, which has a fully functional programming API. For this work, all the programming was carried out in C#. This allowed a full non-linear model to be generated, analysed and post-processed. The stent's surgical deployment and working conditions are simulated in six loading stages:

1. Crimping the stent onto a deflated balloon catheter (a 0.4 mm crimp)
2. Elastic rebound following crimping
3. Expansion of the stent *in vivo* by inflating the balloon (0.4 mm expansion)
4. Elastic rebound following expansion
5. Normal diastolic (80 mmHg) blood pressure loading
6. Normal systolic (120 mmHg) blood pressure loading

The analysis uses an elasto-plastic material model with isotropic linear strain hardening to model the tantalum alloy and full geometric non-linearities (large displacements) are included. A non-linear static solver with arc-length displacement control is used. The allowable normalized residuals are set at 10^{-3} for the force and 10^{-4} for the displacement. The stent's performance is measured by fatigue resistance and radial flexibility.

3.1 Fatigue resistance

Metal fatigue (Duggan and Byrne 1977) involves initial localized fracture leading to irreparable damage and ultimate failure of the structure. Structures like cardiovascular stents, which are subject to large levels of low-intensity cyclical loading, are particularly susceptible. During its lifetime, a stent experiences many millions of alternating blood pressure loadings (approximately 3.8×10^8 over 10 years). Such repetitive loading, even at low stress magnitudes, could eventually cause material fatigue failure.

The *Goodman Plot* is a method of assessing the likelihood of fatigue failure. It is a plot of the mean value of the maximum and minimum stresses during the cyclical loading phase (σ_{mean}) against the magnitude of the difference between them (σ_{amp}), computed at a number of locations. We use the Von Mises measure of stress at every node in the FEM. The *Goodman Line* is the locus of:

$$\frac{\sigma_{\text{mean}}}{\sigma_u} + \frac{\sigma_{\text{amp}}}{\sigma_e} = 1 \tag{5}$$

where σ_e is the material's endurance limit and σ_u is its ultimate strength.

If all the points on the Goodman Plot lie within the Goodman Line (as in Fig. 6), and if the sampling of points is appropriately dense, the structure is deemed safe. Furthermore, the *Goodman Number* (the distance from the line to

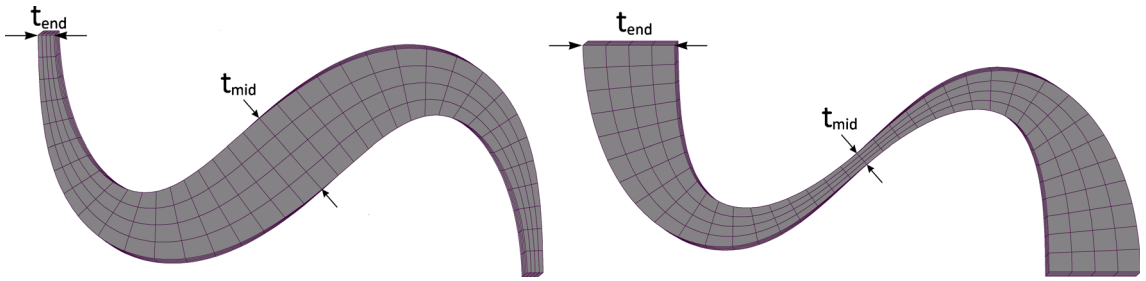

Fig. 7 Varying thickness along the segment's longitudinal direction allows for local control of material distribution

the closest point) is taken as an overall measure of fatigue resistance, FR, to be maximized in design.

$$\mathrm{FR} = \min_i \frac{\left| \frac{\sigma_{\mathrm{mean}}}{\sigma_u} + \frac{\sigma_{\mathrm{amp}}}{\sigma_e} - 1 \right|}{\sqrt{\frac{1}{\sigma_u^2} + \frac{1}{\sigma_e^2}}} \qquad i = 1 \ldots m \tag{6}$$

where m is the number of points at which the Goodman number is plotted.

3.2 Radial flexibility

Stents undergo very large and permanent deformations during deployment, due to the ductile nature of the material. This plastic material behavior allows a stent to be expanded into place within an artery on a balloon-tipped catheter, dilating the artery. Once in place, the expanded stent maintains the opening and reinforces the artery wall.

Restenosis (disease re-occurrence) may occur if the radial flexibility of the stent is too low (i.e., if the stent is too rigid). The challenge is, therefore, to design a stent that is stiff enough to reinforce the artery wall and remain in place after deployment, yet flexible enough to match the flexibility of the surrounding, diseased, artery (Bennett 2003).

In this study, we concern ourselves with the flexibility of the stent under normal working conditions. Radial flexibility, F_{radial}, is determined as the average outward deflection of all nodes under an outward radial force applied to the stent's inner surface and corresponding to 40 mmHg (the difference between assumed diastolic and systolic blood pressures).

Variation in the degree of arterial blockage and, hence, in the radial flexibility of the diseased arteries across patients presents a challenge in design optimization: the target structural performance varies in each clinical case. As described in Section 4.3, we use multi-objective techniques to address this.

4 Structural shape optimization

This section describes the formulation and solution of a multi-objective shape optimization problem based on the developed NURBS modeler and structural performance measures (Sections 1 and 3). After Section 4.1's description of the optimization problem statement, Sections 4.2 and 4.3 present response surface approximations of the true objective functions and the multi-objective Pareto front produced by optimizing over these approximations.

4.1 Problem statement

As discussed in Section 3, a good stent design is highly resistant to fatigue and has a radial flexibility close to that of the diseased artery. The minimum distance to the Goodman line—a measure of a stent's fatigue resistance—is therefore a clear objective to be maximized in design optimization. The target radial flexibility, however, varies from patient to patient with the extent of blood vessel blockage.[1] Our goal is to account for this variability inherent in clinical practice by producing a maximally fatigue-resistant design for a specified blood vessel flexibility. Using established multi-objective optimization techniques to produce a Pareto front in two-objective space is a natural way to achieve this.

Fatigue resistance, FR, and radial flexibility, F_{radial}, as defined in (6) and Section 3.2, are chosen as objective functions to be maximized. The resulting set of Pareto-optimal designs can then be used as a clinical design guide, specifying maximally fatigue-resistant designs for a range of required radial flexibilites. With reference to Sections 2.2 and 2.3, the chosen optimization design variables are the control point weights $w_i, i \in \{1, 2, 3\}$, the thickness variables t_{mid} and t_{end}, and the angle of side slope θ_{side}. These allow for broad variation in three-dimensional shape and in structural performance.

The design variables form the design vector, $\mathbf{x}$:

$$\mathbf{x} = [w_1, w_2, w_3, t_{\mathrm{end}}, t_{\mathrm{mid}}, \theta_{\mathrm{side}}]^{\mathrm{T}} \tag{7}$$

The problem statement is then:

$$\begin{aligned} &\max_{\mathbf{x}} \mathrm{FR}(\mathbf{x}),\ F_{\mathrm{radial}}(\mathbf{x}) \\ \text{subjectto}\ \ &10^{-3} \le w_i \le 10^{2.5} \qquad i \in \{1, 2, 3\} \\ &0.030\ \mathrm{mm} \le t_{\mathrm{end}}, t_{\mathrm{mid}} \le 0.150\ \mathrm{mm} \\ &-10^\circ \le \theta_{\mathrm{side}} \le 10^\circ \end{aligned} \tag{8}$$

The chosen upper and lower bounds on the w_i lead to a wide range of shapes, and the bounds on t_{mid}, t_{end}, and θ_{side} are set to ensure physical feasibility.

4.2 Response surface approximation

Modeling the deployment and working conditions of a stent is a relatively expensive task.

A computer with 6 GB of memory and an *Intel® CORE™ i7-4770* processor takes up to ten minutes to evaluate some stent designs. The tens of thousands of evaluations required for multi-objective optimization make the direct use of this analysis in optimization impractical, motivating the construction of computationally-inexpensive response surface approximations of the two objective functions (Myers et al. 1971). These approximations are denoted $\hat{F}_{\mathrm{radial}(\mathbf{x})}$ and $\hat{\mathrm{FR}}(\mathbf{x})$.

[1] The flexibility of diseased blood vessels is, to the best of the authors' knowledge., not well established in the literature. Certain studies, e.g. Xiang et al. (2008); Shen et al. (2008), indicate values in the range of $[1, 30] \times 10^{-4}$ mm/mmHg.

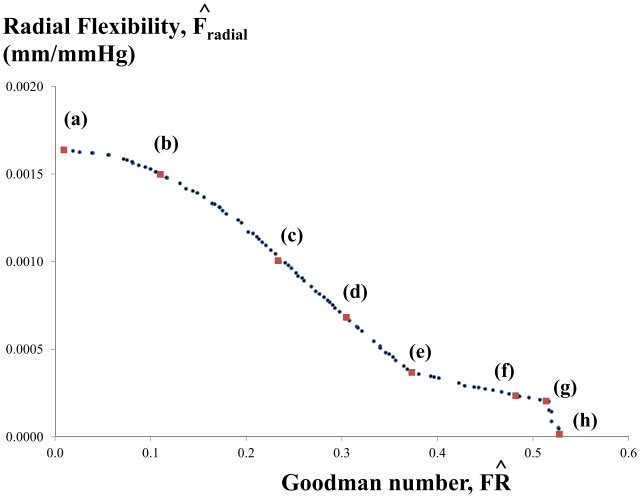

Fig. 8 Along the Pareto optimal front, increasingly flexible stent designs have better fatigue resistance. Figure 9(a)–(h) visualizes shows the annotated results

To fit the response surface, we first randomly generate 140 designs in the 6-dimensional design space using Latin Hypercube sampling (McKay et al. 1979). The structural performance measures—fatigue resistance and radial flexibility—of these 140 designs are calculated as described in Section 3.

Using the *DACE* statistical toolbox (Nielsen et al. 2007), we then fit Kriging response surfaces to each set of design points; the surfaces are used as computationally inexpensive substitutes for the true objective values during optimization. The regression elements of the developed Kriging predictors use quadratic functions and the DACE toolbox's *LIN* correlation function.

The fitted response surfaces have mean squared resubstitution errors which are negligibly far from zero, which we expect given the highly adaptive nature of the Kriging predictors. Average mean-squared errors 2.3×10^{-5} for $\widehat{\mathrm{FR}}(\mathbf{x})$ and 1.1×10^{-3} for $\hat{F}_{\mathrm{radial}}(\mathbf{x})$) under 10-fold cross-validation show that the response surfaces do not unduly over-fit the experimental design data (see Hastie et al. 2005). These low fit errors show that the response surfaces are good approximations of the underlying true objective functions and therefore appropriate for use in optimization.

4.3 Optimization and results

The fitted Kriging response surfaces $\widehat{\mathrm{FR}}(\mathbf{x})$ and $\hat{F}_{\mathrm{radial}}$ replace $\mathrm{FR}(\mathbf{x})$ and F_{radial} in the optimization problem statement of (8). The solution of the quadratic approximation to the underlying problem is, thanks to this replacement, much less computationally expensive than using the true

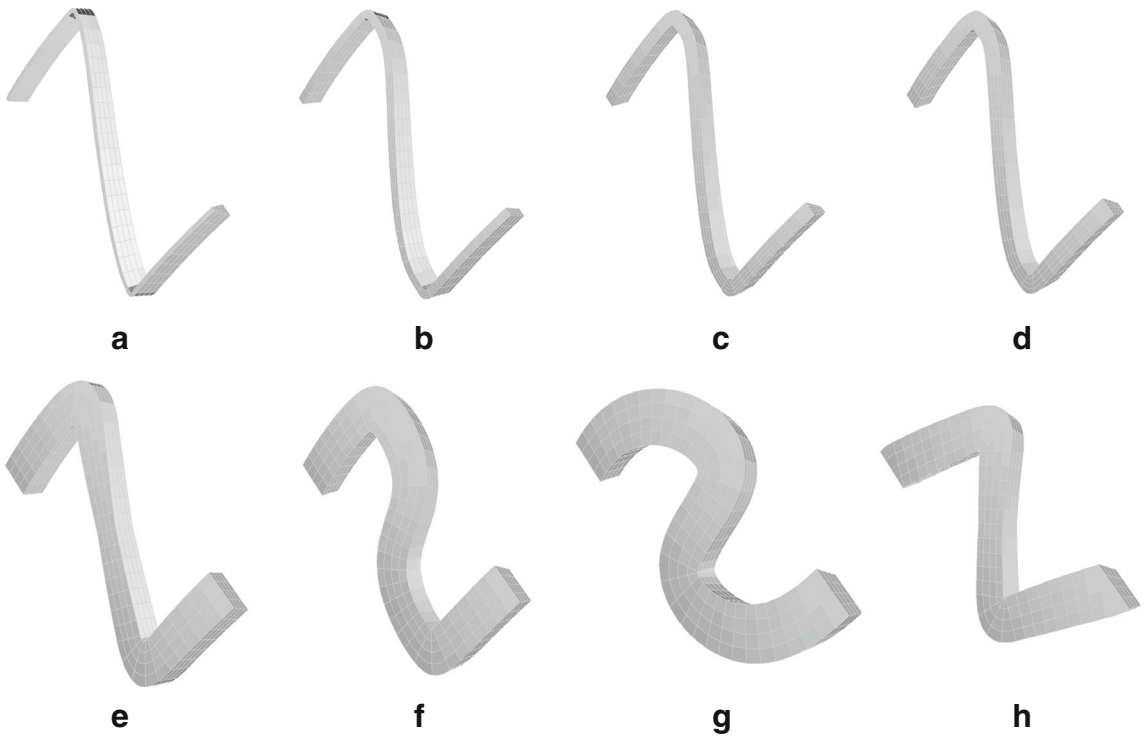

Fig. 9 Selected designs along the Pareto front (Fig. 8). As radial flexibility decreases from design (**a**) to (**h**), fatigue resistance improves and geometry varies widely

Table 1 Design variables for the selected response surface optimization results shown in Fig. 9 (a)–(h)

	w_1	w_2	w_3	t_{end} (mm)	t_{mid} (mm)	θ_{side} (°)
(a)	316.228	0.001	45.107	0.030	0.030	−10.0
(b)	316.092	46.976	39.300	0.030	0.030	−10.0
(c)	316.228	308.389	59.975	0.030	0.035	0.1
(d)	316.156	316.228	4.536	0.055	0.030	10.0
(e)	134.549	9.880	0.278	0.150	0.030	−3.0
(f)	42.289	64.684	300.313	0.150	0.136	7.7
(g)	4.384	22.546	305.088	0.150	0.149	10.0
(h)	0.001	72.272	0.001	0.144	0.030	10.0

performance measures. To solve this multi-objective problem, we use a MATLAB® implementation (Seshadri 2009) of the well-known NSGA-II algorithm (Deb et al. 2002), with a population size of 100 evolved over 1000 generations using binary tournament selection. Crossover and mutation parameters are both set to 20 throughout.

After 1000 generations, the 100 designs in the NSGA-II population converge to the Pareto front shown in Fig. 8. A clear trade-off between the two performance measure emerges; as designs become more flexible (as F_{radial} increases), their resistance to fatigue, $\hat{\text{FR}}$, decreases.

Figure 9 visualizes a small, distributed subset of the Pareto points, as annotated in Fig. 8, and Table 1 shows their design variables. The geometry of the optimal design changes significantly across the multi-objective Pareto front; this demonstrates the proposed NURBS approach's ability to capture a wide range of shapes and its suitability for use in structural shape optimization.

5 Discussion

The response surface-based multi-objective optimization results show a clear trade-off between radial flexibility and fatigue resistance along the Pareto optimal front. Designs with relatively low radial flexibility F_{radial} (e.g., Fig. 9g and h) are highly resistant to fatigue. When the flexibility is high, however, the resulting designs are more susceptible to metal fatigue (e.g., Fig. 9a and b).

Considering the geometry of the optimal stents, this makes intuitive sense. As the designs become less flexible, moving from left to right across Fig. 9, the segment thicknesses, t_{mid} or t_{end}, increase dramatically. Since there is more material available to resist the alternating blood pressure loading, it is reasonable to expect lower stresses and strains, and reduced flexibility.

The selected stents all show pronounced curvature, although the more flexible designs do so to a greater extent.

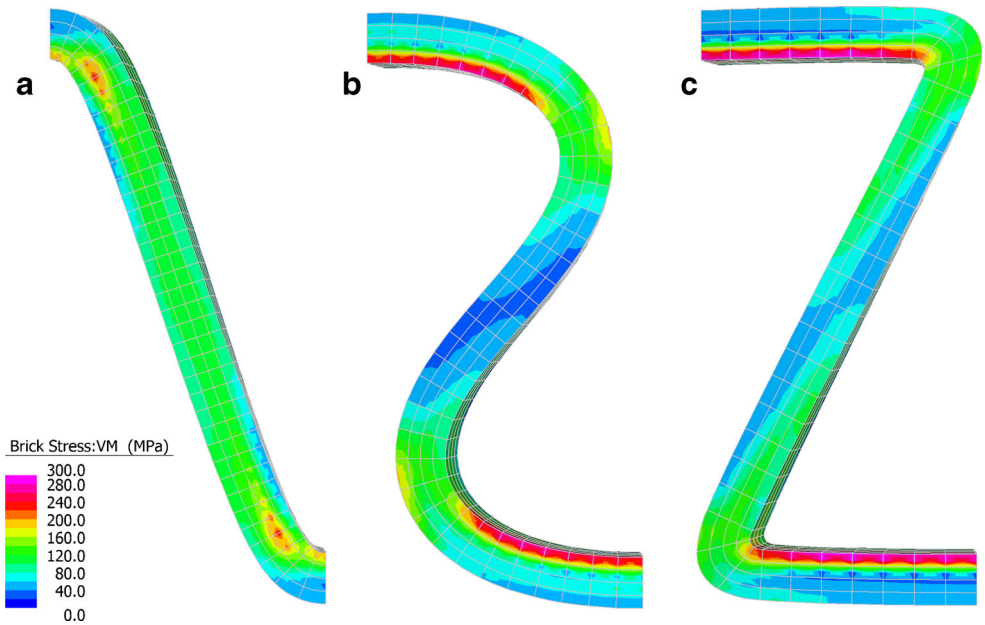

Fig. 10 Fatigue resistance decreases and radial flexibility increases with high local curvature and higher flexibility, as evidenced by plots of von Mises stress at the systolic blood pressure: **a** $FR = 0.45$ & $F_{radial} = 8.8 \times 10^{-5}\ mm/mmHg$; **b** $FR = 0.41$ & $F_{radial} = 1.9 \times 10^{-4}\ mm/mmHg$ and; **c** $FR = 0.32$ & $F_{radial} = 3.1 \times 10^{-4}\ mm/mmHg$. All three stents have a constant thickness of $85\mu mm$

It may well be that the stress concentrations resulting from such curvature are responsible for much of the displacement under the applied pressures and for the relatively low fatigue resistance. The von Mises stress plots in Fig. 10 further detail the reduction in the Goodman number as the flexibility increases. The stress at the systolic blood pressure is a direct measure of the average stress in the Goodman plot. Hence the higher the stress, the lower the Goodman number. The actual Goodman number and flexibility are given for each figure.

The concern with the highly fatigue-resistant designs is their potential to cause restenosis through excessive stiffness. It remains a pressing task for future work to determine suitable target levels of flexibility for inclusion in optimization. Given that an individual artery's degree of blockage contributes to flexibility, the approach we have taken here—designing a maximally fatigue-resistant stent for different radial flexibilities—is most suitable given to its flexibility in adapting design to an individual patient's medical condition.

6 Conclusion

One of this work's main contributions is the use of NURBS control parameters to significantly extend the range of stent shapes that a single geometric modeller can produce. We described a method to use these control parameters as optimization design variables, achieving significant geometric variation compared to previous stent parameterizations. This wide variation ensures we are searching a broad geometric design space during optimization.

Further, the paper introduced a Goodman plot-based measure of fatigue resistance to the optimization problem. Consideration of fatigue resistance and its relationship to other performance metrics is important to maximize the safety of cyclically-loaded stents; we have demonstrated its suitability as an optimization objective function and as a standard measure of stent performance for future research in this area.

Rather than seeking a single optimal design, the use of multi-objective optimization addresses the uncertainty in the radial flexibility requirements of a stent. The resulting Pareto set forms the basis of a design guide from which physicians can select an appropriate fatigue-resistant design depending on the characteristics of a particular patient's diseased artery.

Continuing this work, we will explore the use of other NURBS parameters besides control weights as design variables, with the goal of generating even more diverse geometries. Extending our physical model to include the artery wall and the blockage at the diseased site will allow us to consider other performance measures, and to analyze the trade-offs between them in a multi-objective formulation. We also intend to explore the use of stochastic optimization methods, although the computational expense of our objective and constraint functions, and the many required evaluations, may be prohibitive.

Acknowledgments The authors wish to thank Dr. Brendan Cunniffe, formerly of Medtronic Vascular, Galway, Ireland, for his help on this project.

References

Atherton MA, Bates RA (2004) Robust optimization of cardiovascular stents: a comparison of methods. Eng Optim 36(2):207–217

Balcon R, Beyar R, Chierchia S, De Scheerder I, Hugenholtz PG, Kiemeneij F, Meier B, Meyer J, Monassier JP et al (1997) Recommendations on stent manufacture, implantation and utilization. Eur Heart J 18:1536–1547

Bennett MR (2003) In-stent stenosis: pathology and implications for the development of drug eluting stents. Heart 89(2):218–224

Deb K, Pratap A, Agarwal S, Meyarivan T (2002) A fast and elitist multiobjective genetic algorithm: NSGA-II. IEEE Trans Evol Comput 6(2):182–197

Duggan TV, Byrne J (1977) Fatigue as a design criterion, vol 77. Macmillan, London

Dumoulin C, Cochelin B (2000) Mechanical behaviour modelling of balloon-expandable stents. J Biomech 33(11):1461–1470

Etave F, Finet G, Boivin M, Boyer JC, Rioufol G, Thollet G (2001) Mechanical properties of coronary stents determined by using finite element analysis. J Biomech 34(8):1065–1075

Harewood F, Thornton R, Ireland M, Sharp P (2011) Step change in design: exploring sixty stent design variations overnight. Altair Product Design Workshop

Hastie T, Tibshirani R, Friedman J, Franklin J (2005) The elements of statistical learning: data mining, inference and prediction. Math Intell 27(2):83–85

Kelliher D, Clune R, Campbell JS, Robinson JC, Appelbe B, Buttimer C (2008) Sensitivity of shape change on the performance of stainless steel cardio-vascular stents. In: Proceedings of the 7th ASMO UK conference on engineering design optimization, Bath, pp 274–283

Lally C, Dolan F, Prendergast PJ (2005) Cardiovascular stent design and vessel stresses: a finite element analysis. J Biomech 38(8):1574–1581

Li N, Zhang H, Ouyang H (2009) Shape optimization of coronary artery stent based on a parametric model. Finite Elem Anal Des 45(67):468–475

McKay MD, Beckman RJ, Conover WJ (1979) Comparison of three methods for selecting values of input variables in the analysis of output from a computer code. Technometrics 21(2):239–245

Migliavacca F, Petrini L, Colombo M, Auricchio F, Pietrabissa R (2002) Mechanical behavior of coronary stents investigated through the finite element method. J Biomech 35(6):803–811

Myers RH, Montgomery DC, Anderson-Cook CM (1971) Response surface methodology. Allyn and Bacon, Boston

Nielsen HB, Lophaven SN, Sondergaard J (2007) DACE: a matlab kriging toolbox. http://www2.imm.dtu.dk/hbni/dace/

Pant S, Bressloff NW, Limbert G (2011a) Geometry parameterization and multidisciplinary constrained optimization of coronary stents. Biomech Model Mechanobiol 11(1–2):61–82

Pant S, Limbert G, Curzen NP, Bressloff NW (2011b) Multiobjective design optimisation of coronary stents. Biomaterials 32(31):7755–7773

Piegl LA, Tiller W (1997) The NURBS book. Springer Verlag
Qian X (2010) Full analytical sensitivities in NURBS based isogeometric shape optimization. Comput Methods Appl Mech Eng 199(29):2059–2071
Serruys PW (2001) Handbook of coronary stents. Recherche 67:02
Seshadri A (2009) NSGA - II: a multi-objective optimization algorithm - MATLAB file exchange., http://www.mathworks.com/matlabcentral/fileexchange/10429-nsg a-ii-a-multi-objective-optimization-algorithm
Shen X, Yi H, Ni Z (2008) Effects of stent design parameters on radial force of stent. In: The 2nd international conference on bioinformatics and biomedical engineering. ICBBE 2008, IEEE, pp 1712–1716
Timmins L, Moreno M, Meyer C, Criscione J, Rachev A, Moore J (2007) Stented artery biomechanics and device design optimization. Med Biol Eng Comput 45(5):505–513
Wu W, Yang DZ, Huang YY, Qi M, Wang WQ (2008) Topology optimization of a novel stent platform with drug reservoirs. Med Eng Phys 30(9):1177–1185
Xiang S, Hong Y, Zhonghua N, Xingzhong GU (2008) Optimization of coronary stent structure design for maximizing the anti-compression mechanical property. Chin J Mech Eng 21(6)